PERGAMON

Chemical Engineering Science 54 (1999) 4007–4022

Chemical Engineering Science

Bubble size distribution and coarsening of aqueous foams

S.A. Magrabi, B.Z. Dlugogorski*, G.J. Jameson

ARC Research Centre for Multiphase Processes, Department of Chemical Engineering, The University of Newcastle, Callaghan, NSW 2308, Australia

Received 28 September 1998; received in revised form 12 January 1999; accepted 24 January 1999

Abstract

This paper characterises the bubble size distribution of aqueous foams, produced by a compressed-air foam generator. The time evolution of bubble size distribution in aqueous foams is experimentally measured using a CCD video camera. A computer model, which predicts the change in bubble size distribution with time, is used to simulate the coarsening and disproportionation of aqueous foams. As an extension of previous computer simulations, our model incorporates the variation in liquid fraction during the foam aging process, thereby enabling the simulation of both wet and dry foams. It is found that a Weibull-type distribution best approximates the narrow bubble-size distribution produced by a compressed-air foam generator. The modelled predictions show good agreement with the experimental measurements and a sensitivity analysis indicates a significant dependence of the model on drainage (hence on the thickness of the lamellae), the Henry constant, the gas diffusivity and the surface tension of the foam solution.

Keywords: Foam; Diffusion; Mass transfer; Bubble growth; Coarsening; Fire fighting

1. Introduction

Aqueous foams are non-equilibrium dispersions of gas bubbles in a relatively smaller volume of liquid. Soap froths, crude oil foams, shaving foams and fire-fighting foams are all common occurrences of foam products in our daily lives. Aqueous foams are intrinsically non-equilibrium materials, in that their properties vary with time as a result of shifts in the distribution of gas and liquid phases. For instance, when fire-fighting foams are used as barriers to thermal radiation in fire mitigation, they are placed well in advance of the approaching fire. Hence, the foam ages with time until the fire approaches, resulting in a change in its bubble morphology and gas–liquid fraction.

The rheology and stability of the foam are strongly influenced by the foam's bubble size distribution and gas–liquid fraction, as highlighted in numerous studies in the literature. For example, Rand and Kraynik (1983) have described a relation between the bubble-size distribution and the rate of drainage. The enhanced stability of foams with smaller bubbles was explained by a decrease of drainage. Sarma and Khilar (1988) reported that a more uniform bubble size distribution and high initial gas volume fraction gave more stable foams. Hence, the discernment of the bubble-size distribution in a foam is essential for an improved understanding of the foam properties and the stability of those properties. Moreover, changes in bubble size distribution can be used to distinguish between the physical processes that contribute to the transformation of foam properties.

The purpose of this study is threefold: firstly, to characterise the bubble morphology of compressed-air foams (CAF), since compressed-air foam generation is a newly developed method of foam production as opposed to the traditional method of foam generation by gas aspiration or sparging. Secondly, to highlight and contrast the difference in bubble size distribution between compressed-air foams and other foams studied previously. Thirdly, to age the foam and study the time evolution of bubble-size distribution. This includes modelling the coarsening and disproportionation of compressed-air foams and comparing them with empirical measurements. An extended Lemlich (1978) model is applied in the computer simulations.

* Corresponding author. Tel.: + 61-2-4921-6176; fax: + 61-2-4921-6920.

E-mail address: cgbzd@alinga.newcastle.edu.au (B.Z. Dlugogorski).

0009-2509/99/$ - see front matter
PII: S0009-2509(99)00098-6

2. Experimental

2.1. Apparatus

Aqueous foams are traditionally generated by the air-aspiration or sparging of foam solution at the point of application (Bikerman, 1973; Stavans, 1990; Gandolfo and Rosano, 1997). Lately, in certain applications like fire-fighting and enhanced oil recovery, these air-aspirated foams are being replaced by compressed-air foams (CAFs) due to their superior performance (Liebson, 1991).

In this study, we use compressed-air foam which is made by injecting compressed air into a surfactant solution at a pressure of 580 kPa (gauge) in a foam generator described previously (Magrabi et al., 1997; Gardiner et al., 1998a). A schematic illustration of the foam generator is shown in Fig. 1. Compressed air at 580 kPa (gauge) is used to force the foam solution out of the pressure vessel. Subsequently, the foam solution is combined with compressed air in an in-line mixer, which leads to the foam improver. Compacted steel wool placed in the T-junction constitutes the in-line mixer. The foam improver incorporates 10 m of 12.7 mm diameter flexible tubing, to induce mixing, in order to improve foam quality. The foam solution is prepared by diluting a 3% generic aqueous film forming fire-fighting-foam concentrate with 97% deionised water. The composition of the foam concentrate is listed in Table 1. The liquid fraction in the generated foam is determined by using the flowmeter readings and verified by weighing the foam at atmospheric pressure as prescribed by NFPA-412 (1993).

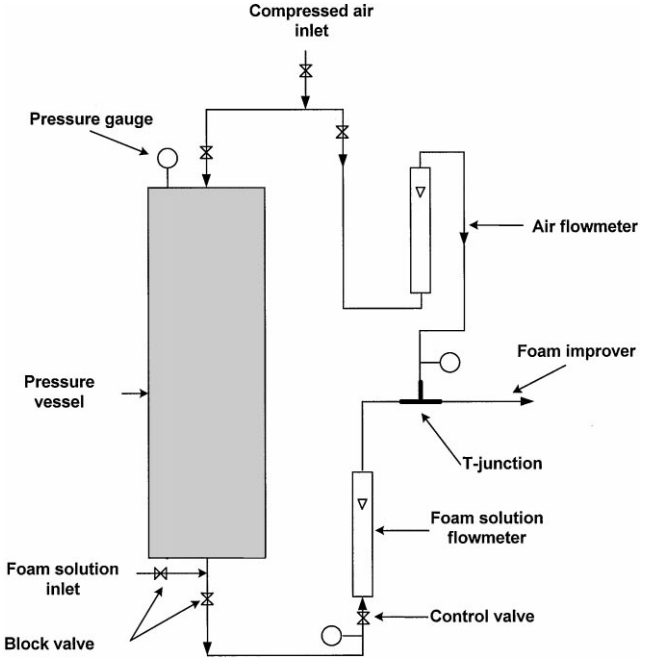

Fig. 1. Schematic diagram of the compressed-air foam generator.

Table 1
Composition of the foam concentrate. This concentrate was mixed with water in the volume ratio of 3:97 before being aerated with compressed air

Chemical	Trade name	% by weight	Function
1 Fluoro-alkyl surfactant	FC-100	12	Surfactant
2 Phenyl sulphate surfactant	Triton X-305	11	Surfactant
3 Sodium octyl sulphate	–	13	Surfactant
4 Diethylene otycol monobutyl ether	–	9	Stabiliser
5 Water	–	55	Solvent

2.2. Procedure

A variety of techniques have been developed to study bubble size distribution: the conductivity probe (Lewis et al., 1984), the optical fibre-based method (Bisperink et al., 1992), light transmission procedures (Durian et al., 1991; Lachaise et al., 1991) and photographic methods (Calvert and Nezhati, 1986; Kroezen and Wassink, 1987; Tam et al., 1997) to mention a few. Photographic methods are non-intrusive and have the advantage of keeping the cell size distribution unchanged and eliminating any distortions caused by introducing probes. In this study, video microscopy, which couples a CCD camera to an objective microscopic lens, was utilised to capture the evolution of bubble size profiles with time.

Freshly generated foam was placed in a photography cell, which is comprised of a cubicle chamber ($100 \times 100 \times 100$ mm) made of perspex. A microscopic graticule with a 1 mm grid was embedded on the front face of the photography cell, for scaling purposes. A CCD video camera fitted with an objective lens transferred the bubble images to a video recorder. The cell was illuminated from the sides and the rear to enhance the contrast between the gas phase in the bubbles and the liquid in the films between the bubbles. An image analysis package, *Optimas*, was used to process the captured bubble images. The initial bubble size distribution was measured in freshly generated foam of liquid fraction φ of 0.2, 0.1, 0.05 and 0.033. The foam was then allowed to age and the bubble size distribution was measured at 60, 240, 480, 960 and 1920 s after generation.

The bubble frequency distribution measured photographically at a transparent surface will be different from the bubble size distribution in the bulk of the foam, because the plane of view discriminates statistically against the inclusion of small bubbles (de Vries, 1972; Cheng and Lemlich, 1983). This statistical bias can be corrected by the following relationship

$$F(r) = \frac{f_s(r)}{r} \int_0^\infty rF(r)\,\mathrm{d}r, \tag{1}$$

where $F(r)$ is the true frequency size distribution in the bulk of the foam and $f_s(r)$ is the observed frequency size distribution at the transparent surface. The average diameter r_{10} can then be calculated from

$$r_{10} = \int_0^\infty rF(r)\,\mathrm{d}r. \tag{2}$$

Furthermore, de Vries (1972) shows that

$$\frac{1}{r_{10}} = \int_0^\infty \frac{f_s(r)}{r}\,\mathrm{d}r, \tag{3}$$

In carrying out the correction, we first calculate r_{10} from Eq. (3) and then eliminate the integrals between Eqs. (2) and (1) to obtain $F(r)$ from $(f_s(r)/r)r_{10}$. Other errors highlighted by Cheng and Lemlich (1983) such as bubble distortion and bubble segregation were ignored in the present work as done by others (Kroezen and Wassink, 1987).

In addition to the bubble size, the time evolution of the liquid fraction in the foam was experimentally determined by using the sonic velocity method (Gardiner et al., 1998b). This approach encompasses the relationship proposed by Wood (1941) for the velocity of sound through a mixture. By treating a foam as a mixture composed of a compressible gas satisfying the ideal gas law, and an incompressible liquid, and neglecting the bubble response to acoustics, the velocity of sound in a foam v can be related to the liquid fraction φ by

$$v^2 = \frac{\gamma P_a}{\rho_l}\left(\frac{1}{\varphi(1-\varphi)}\right), \tag{4}$$

where $\gamma = C_p/C_v$ for the isentropic expansion of an ideal gas. The sonic velocity was measured by immersing two microphones and a speaker into the foam sample and using an oscilloscope to measure the time delay between the detection by the microphones of a square pulse (frequency ≈ 3400 Hz) produced by the speaker.

3. Modelling the evolution of bubble size distribution in foams

Monsalve and Schechter (1984) developed a bubble population balance by considering a bubble size distribution function $F(r,t)$. $F(r,t)$ was defined such that $F(r,t)\,\mathrm{d}r$ is the total number of bubbles at time t having equivalent spherical radii that lie within the range r to $r+\mathrm{d}r$. They demonstrated that F evolves according to the following conservation equation:

$$\frac{\partial F}{\partial t} + \frac{\partial}{\partial r}(\psi F) = 0, \tag{5}$$

where $\psi(r,t)$ is the rate at which the bubble radius r at time t, changes with time. The specific functional form for $\psi(r,t)$ used in Eq. (5) was deduced by Lemlich (1978) and predicts changes in bubbles size distribution due to inter-bubble gas diffusion in foam. It can be written as

$$\psi(r,t) = \frac{\mathrm{d}r}{\mathrm{d}t} = \frac{2J\sigma R_g T}{P_a}\left(\frac{\int_0^\infty rF(r,t)\,\mathrm{d}r}{\int_0^\infty r^2F(r,t)\,\mathrm{d}r} - \frac{1}{r}\right), \tag{6}$$

where σ denotes the surface tension, T is the absolute temperature, P_a stands for the atmospheric pressure, R_g is the universal gas constant and J is the effective permeability coefficient. Eq. (6) can be written more concisely as

$$\frac{\mathrm{d}r}{\mathrm{d}t} = \psi(r,t) = K\left(\frac{1}{r_{21}} - \frac{1}{r}\right), \tag{7}$$

where $K = 2J\sigma R_g T/P_a$ and

$$r_{21} = \left(\frac{\int_0^\infty r^2F(r,t)\mathrm{d}r}{\int_0^\infty rF(r,t)\,\mathrm{d}r}\right). \tag{8}$$

The partial differential equation suggested by Monsalve and Schechter (1984) in Eq. (5) describes the time evolution of the bubble size distribution $F(r,t)$. For an arbitrary initial size distribution, $F(r,0)$, the analytical solution of Eq. (5) cannot be obtained except for two limiting cases, namely, a narrow size distribution and for asymptotically large times as described by Markworth (1985). Numerically, it is easier to solve a set of ordinary differential equations describing the evolution of the radial bubble size according to Eq. (6), constrained by the total amount of gas present in the foam. For this reason, the numerical approach which corresponds to that developed by Lemlich (1978) is followed in this study.

The Lemlich (1978) model assumes that the gas diffuses from a real bubble to a virtual bubble. The virtual bubble is located at the centreline of a lamella between adjacent real bubbles everywhere in the foam. The role of the virtual bubble is to serve as a reservoir of dissolved gas diffusing from bubbles whose radii are less than r_{21}. The gas is then redistributed by the liquid in the lamellae and the Plateau borders and then transferred to all the bubbles whose radii exceed r_{21}. The mass transfer among the bubbles is governed by Eq. (6); its derivation is presented in the appendix.

The effective permeability to gas transfer J in Eq. (8) is the reciprocal of the sum of the interfacial resistance, $1/h$, and the liquid resistance, $f/(2DH)$,

$$\frac{1}{J} = \frac{1}{h} + \frac{f}{2DH}, \tag{9}$$

where H is Henry's constant, D is the diffusivity and f is the average film thickness between adjacent bubbles. In most foams, the lamella thickness is statistically of the order of 10^{-6} m (de Vries, 1972). Consequently, the interfacial resistance can be ignored, as it is negligible compared to the liquid layer resistance. For spherical

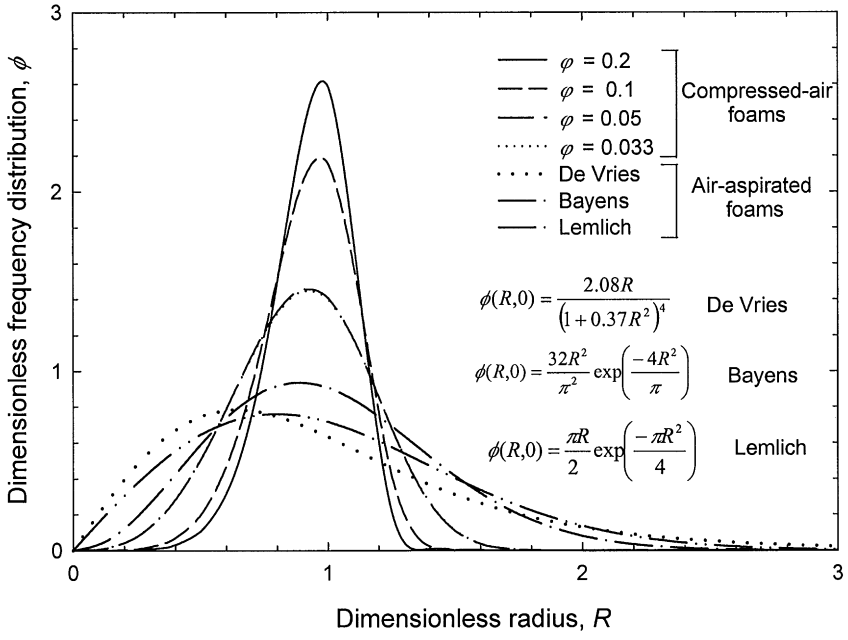

Fig. 2. Plot of dimensionless frequency distribution ϕ against dimensionless radius R, showing the narrower initial bubble size distribution in compressed-air foams in contrast to air-aspirated foams used in previous studies. The distribution parameters for the compressed-air foams are listed in Table 2.

bubbles, the following expression can be derived for the effective permeability J:

$$J = \frac{3DH(1-\varphi)}{\varphi r_{32}}, \tag{10}$$

where φ is the volumetric fraction of liquid in the foam (Lemlich, 1978). As foam bubbles have a dodecahedral shape the spherical coefficient of 3 in Eq. (10) is changed to a regular dodecahedral coefficient of 3.3 (Manegold, 1953).

For solution purposes, Eq. (6) was transformed into the following dimensionless form:

$$\frac{\mathrm{d}R}{\mathrm{d}\tau} = \kappa\left(\frac{1}{R_{21}} - \frac{1}{R}\right), \tag{11}$$

where the dimensionless radius $R = r/r_c$, the dimensionless time $\tau = t/(r_c^2/D)$, and the dimensionless parameter $\kappa = K/D$. Subsequently, the fifth-order Runge–Kutta method was exploited to solve Eq. (11). The initial conditions are given by the initial bubble size distribution which is empirically measured; see Fig. 2 for $F(r)$ at $t = 0$.

In the modelling, the probability density function representing the initial bubble size distribution is discretised into several hundred equally spaced class intervals, with a frequency given by the dimensionless frequency distribution function $\phi\,[\phi = r_i F(r)]$, where r_i is the initial arithmetic mean radius given by

$$r_{10}(0) = \int_0^\infty rF(r,0)\,\mathrm{d}r. \tag{12}$$

At each time step, a set of ordinary differential equations describing the evolution of the bubble radii [Eq. (11)] is solved simultaneously for all class intervals. It follows from the model that the bubbles of radius r, in a certain class interval, grow if $r > r_{21}$ and shrink if $r < r_{21}$. In addition, if the bubble radius r in a certain class interval approaches a critical limit (approximately $0.1r_{21}$ at $t = 0$) the class interval is subsequently removed.

After each time step the bubble radius r changes (increases or decreases) as governed by Eq. (7), leading to a change in the width of the class intervals. Therefore, the frequency distribution in each class interval is changed (increased or decreased) proportionally to the new width of the class interval and the class mark is shifted to the midpoint of the revised class interval. Furthermore, the frequency in each class interval is normalised such that $\int_0^\infty \phi(R)\,\mathrm{d}R = 1$ and the total volume of gas in the foam is conserved. Since the frequency distribution function and liquid fraction in the foam change after each time step, the recalculated R_{21} and r_{32}, along with the experimentally measured liquid fraction, is incorporated into the model at successive time steps.

4. Results and discussion

4.1. Characteristics of compressed-air foams

Fig. 2 depicts the contrast in the initial bubble size distribution between air-aspirated foams used in

previous studies and the compressed-air foams used in our work. The dimensionless frequency distribution parameter ϕ is plotted against the dimensionless radius R ($R = r/r_i$). The critical radii r_i for the various compressed-air foams ($\varphi = 0.2, 0.1, 0.05, 0.033$) are 65, 81.8, 120 and 121 μm, respectively.

The compressed-air foams ($\varphi = 0.2, 0.1, 0.05, 0.033$) are characterised by a narrower bubble size distribution than the gas-aspirated foams generated by de Vries (1957), Gal-Or and Hoelscher (1966) and Lemlich (1982). This observed difference can be ascribed to the method of foam generation utilised in this study. With reference to Fig. 1, the combination of compressed-air and foam solution in the in-line mixer, results in foam being produced by the shearing action between the air–foam concentrate solution and the compacted steel wool. The resulting foam portrays a narrow bubble size distribution and demonstrates greater stability due to a reduced coarsening rate.

During the analysis of the captured bubble images, the image processing software computes the area-equivalent diameter d_b from the cross-sectional area of the bubbles in the sample. On the basis of the area-equivalent diameter d_b, the bubbles were divided into classes of 40–60 μm increments. The bubble size data were then plotted on a cumulative frequency basis on both arithmetic and logarithmic probability scales in order to fit a statistical approximation which best represents the bubble size distribution in the foam sample. The chi-square compatibility criterion (Himmelblau, 1970), known as the goodness-of-fit test, was used to compare the empirical bubble distribution and three statistical distributions: normal, log-normal and Weibull (1951). A significance level of 0.05 was selected in the analysis, implying 95% confidence that the right decision is made in either accepting or rejecting the null hypothesis. The goodness-of-fit test showed that the bubble size distribution of the foams under study is best approximated by a Weibull-type distribution of the following form:

$$F(r) = \frac{\alpha}{\beta^{\alpha}} r^{\alpha-1} \, \mathrm{e}^{-(r/\beta)^{\alpha}}, \tag{13}$$

where α and β are statistical distribution parameters, and $F(r)$ is the frequency distribution function. Table 2 shows the statistical distribution parameters for the initial bubble size distributions in compressed-air foams of varying liquid fraction; see Fig. 2. A broader bubble size distribution was observed with increasing liquid fraction.

Table 2
Weibull statistical distribution parameters for the initial bubble size distribution of compressed-air foams of varying liquid fraction

Liquid fraction φ	α	β
0.2	7.0 ± 0.7	129.7 ± 1.4
0.1	5.9 ± 0.2	170.1 ± 0.9
0.05	3.8 ± 0.1	244.0 ± 1.5
0.033	3.8 ± 0.2	263.8 ± 2.5

Fig. 3 illustrates the change in bubble size distribution with time during the aging of a foam of liquid fraction $\varphi = 0.2$. In addition, the figure demonstrates the Weibull distribution functions and the empirically measured

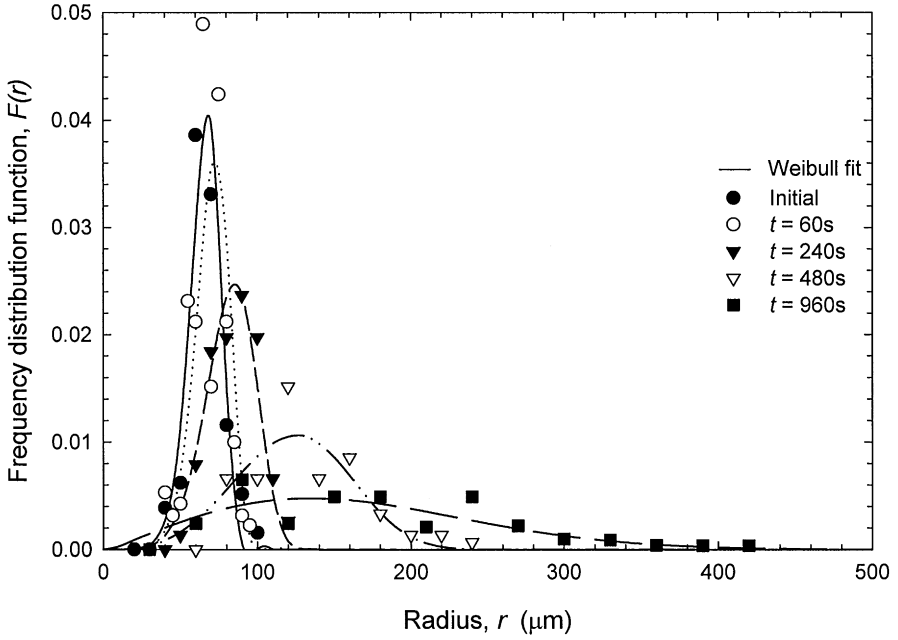

Fig. 3. The Weibull distribution function shows a satisfactory fit to the measured bubble size distributions in compressed-air foams. The measured and expected bubble size distributions were compared with the chi-square test at a significance level of 0.05.

bubble distributions. Note that in previous studies (Calvert and Nezhati, 1986; Lachaise et al., 1991; de Icaza et al., 1994) the log-normal distribution provided the best fit to approximate the distribution of bubbles in a foam. This difference can be ascribed to the method of foam generation which results in a narrower bubble distribution as discussed in previous sections of this paper.

4.2. The time evolution of bubble size distribution in aqueous foams

Foams age by an assortment of processes encompassing the drainage of liquid from the films separating the foam bubbles, the coalescence of adjacent bubbles due to the rupture of the film encapsulating the bubbles and foam coarsening driven by the diffusion of gas from smaller to larger bubbles. Fig. 4 shows the contrast in a drier foam ($\varphi = 0.05$), between the modelled and empirical results for the time evolution of bubble size distribution. Similarly, Fig. 5 illustrates the observed and simulated bubble distributions in a wet foam ($\varphi = 0.2$). In both these cases, the modelled results were obtained by using Lemlich's (1978) approach, whereby a constant liquid volume fraction equivalent to the initial liquid fraction was assumed throughout the simulations, allowing no drainage and thinning of the lamellae. At the outset, the model was initiated by feeding in the empirical measured bubbles size distribution of a freshly generated foam. It is seen that there is a marked discrepancy between the experimental results and those predicted by the simulation.

Our experimental observations showed that the liquid fraction in a foam decreases considerably with time during the aging process, as manifested by Fig. 6. As anticipated, the liquid fraction in the wetter foam ($\varphi = 0.2$) shows a dramatic reduction in its liquid holdup φ from 0.2 to 0.002 in 1920 s. The drier foam ($\varphi = 0.05$) on the contrary shows a comparatively gradual decline in its liquid hold-up.

The average lamella film thickness f is a function of the liquid volume fraction in the foam. During the aging process, the foam loses its liquid fraction due to film and gravitational drainage. In addition, the bubble size also increases due to Ostwald ripening. The amalgamation of these factors results in a reduction in the film thickness, leading to the shortening of the diffusional path for gas transfer between adjoining bubbles. This parameter may not be significant whilst modelling very dry foams. Very dry foams have a small liquid hold-up and exhibit little or no drainage. This implies that the film thickness displays almost no change. In contrast, the larger liquid hold-up and consequently larger drainage rates in wet foams imply that the film thickness shows a marked contraction as the foam ages. Hence, the diffusional path is considerably shortened and the variation of the lamellae thickness needs to be taken into account in the model for inter-bubble gas diffusion.

Fig. 7 illustrates the bubble size distribution predicted by our model for a wet foam ($\varphi = 0.2$). The model incorporates the liquid loss from the foam due to drainage, given by Fig. 6. An improved accord was observed between the experimental and simulated results highlighting the importance of incorporating the reduction in the liquid fraction due to drainage. The profound effect of foam drainage on the modelled bubble size profiles is

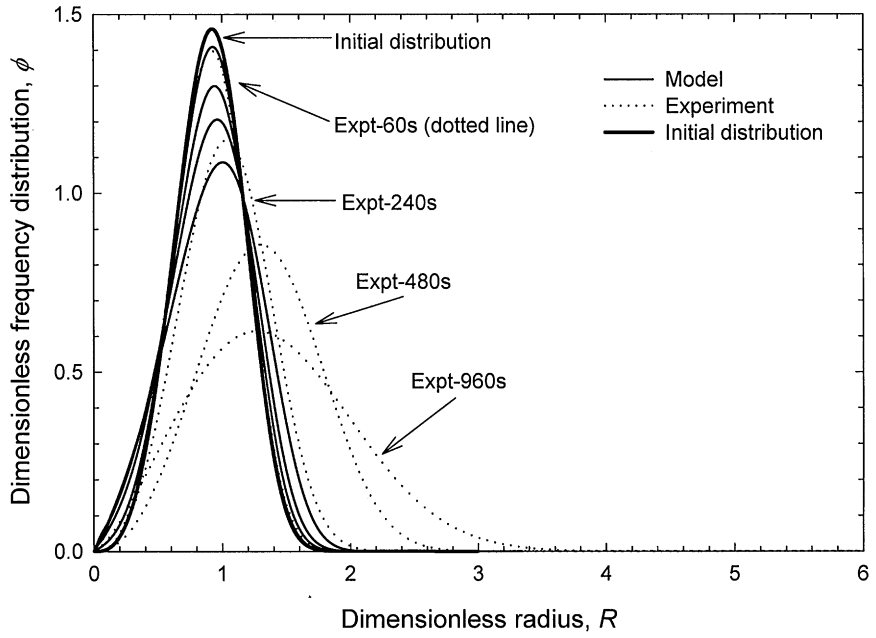

Fig. 4. Modelled (constant liquid fraction) and empirical results for the time evolution of bubble size distribution in the drier foam ($\varphi = 0.05$). The graph illustrates the measured and predicted bubble size profiles at 60, 240, 480 and 960 s.

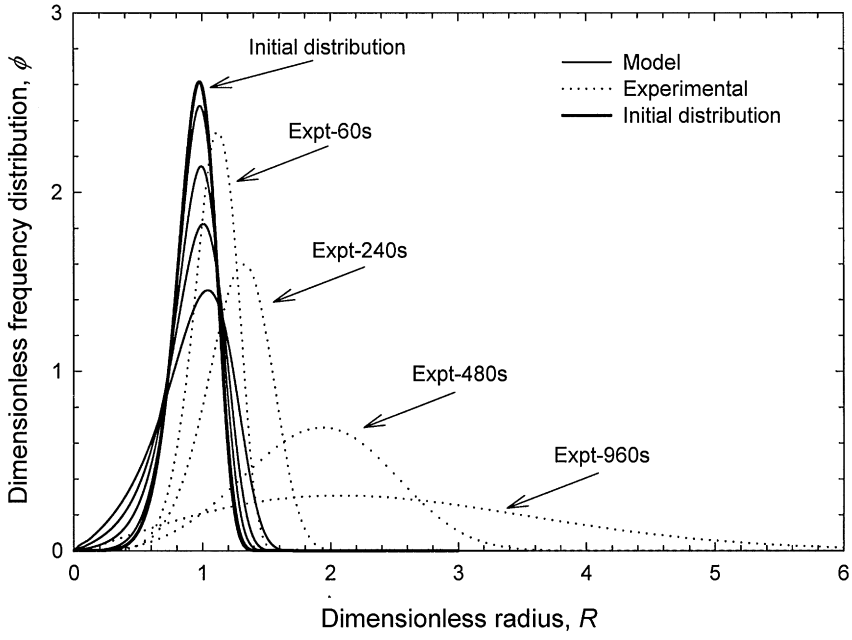

Fig. 5. Simulated (constant liquid fraction) and empirical results for the time evolution of bubble size distribution in a wet foam ($\varphi = 0.2$) at 60, 240, 480 and 960 s.

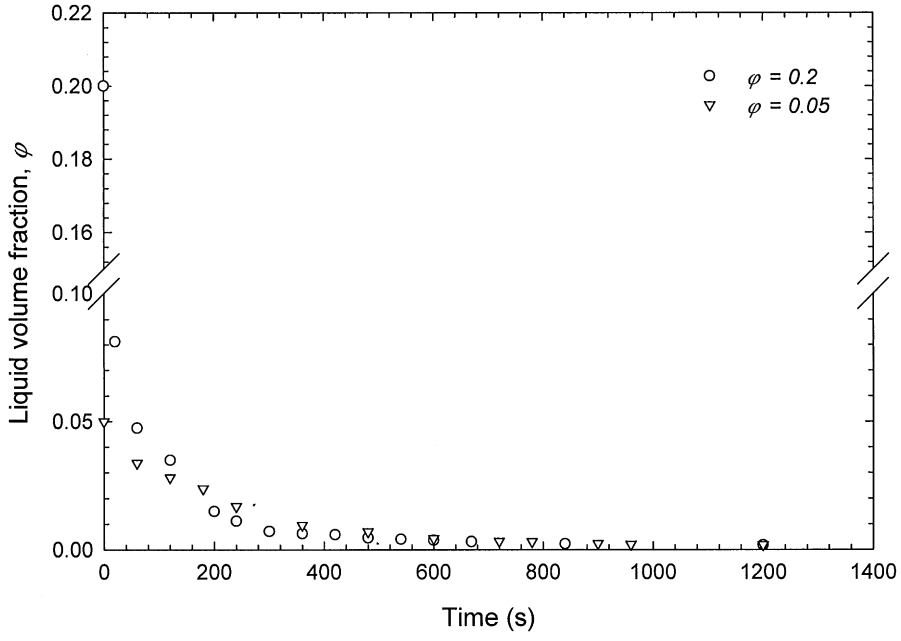

Fig. 6. The time evolution of liquid fraction in a wet ($\varphi = 0.2$) and drier foam ($\varphi = 0.05$). The wet foam exhibits a dramatic reduction in its liquid holdup in contrast to the gradual decline shown by the drier foam.

manifested by comparing the simulation results in Figs. 5 and 7. In effect, the model recalculates the liquid volume fraction in the foam at each time step with reference to Fig. 6, adjusting the effective permeability to gas transfer J in Eq. (10). This in turn results in a proportional increase in the modelling parameter κ in Eq. (11), which has a significant bearing on the solution of the system of ordinary differential equations.

Fig. 8 illustrates the bubble size distribution predicted by our model for a drier foam ($\varphi = 0.05$). As in the case of the wet foam ($\varphi = 0.2$) the empirical and computer-simulated bubble size distributions show improved agreement once drainage is taken into account in the simulations. However, the change in the bubble size distribution function for drier foams once the drainage is included in the simulation is not as significant as for wet

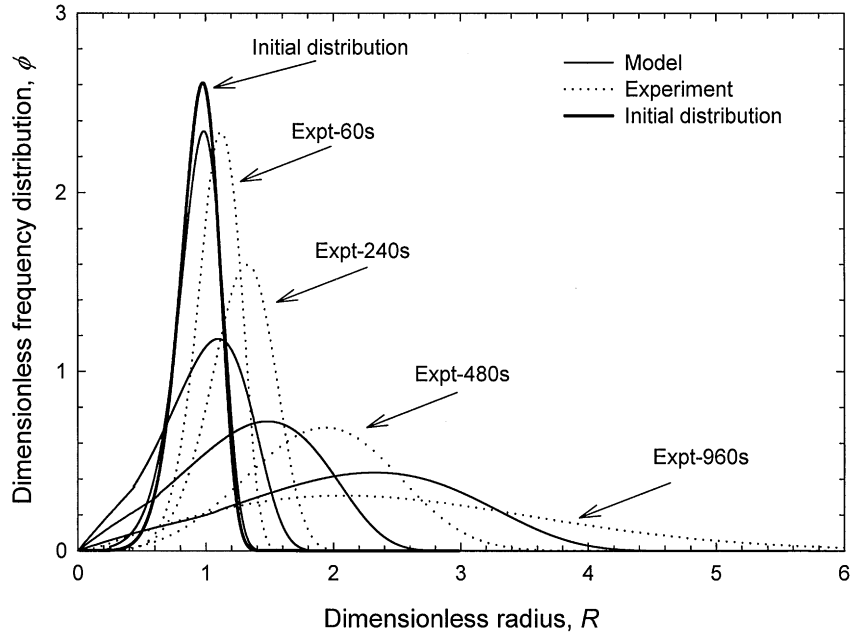

Fig. 7. The effect of incorporating drainage in the simulation of a wet foam ($\varphi = 0.2$). The plot illustrates the evolving bubble size distribution in a wet foam at 60, 240, 480 and 960 s, respectively.

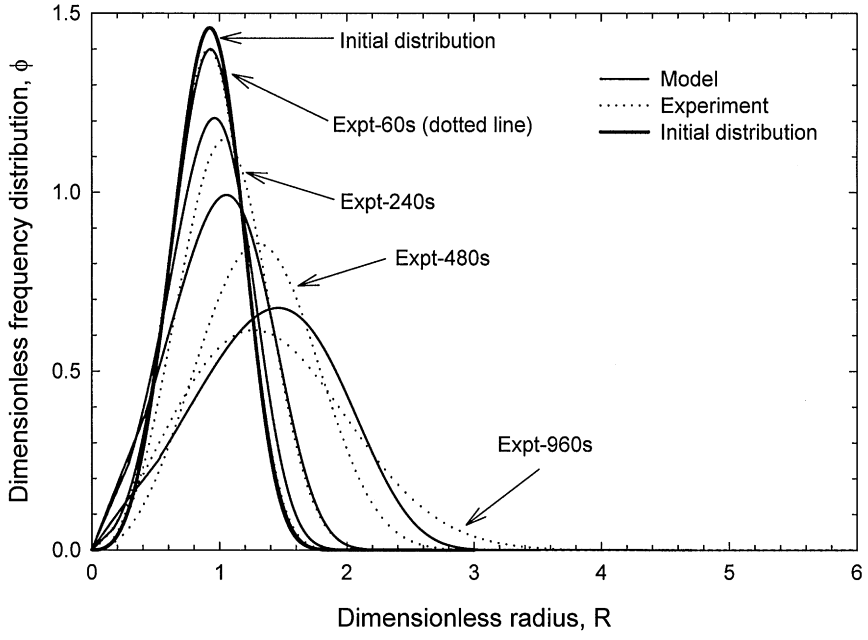

Fig. 8. The evolving bubble size profile in the drier foam ($\varphi = 0.05$). An illustration of the modelled (incorporating the changing liquid fraction) and empirical results at 60, 240, 480 and 960 s, respectively.

foams. This is because in the drier foam ($\varphi = 0.05$) only a relatively small amount of liquid can drain.

4.3. Bubble growth and coarsening in aqueous foams

The coarsening observed in foams is analogous to grain growth in metals, which is governed by von Neumann's (1952) law. A pattern in either two or three dimensions is in a scaling state if all of its distribution and correlation functions for all dimensionless quantities are constant in time (von Neumann, 1952). In foams, the only pattern property that can vary is the mean length scale of the bubbles, e.g. the radius. Using von Neumann's law, it is can be shown that the mean bubble radius r grows as a power law during the scaling state, i.e. $r \propto t^{\chi}$, where $\chi = 0.5$ (Glazier and Weaire, 1992).

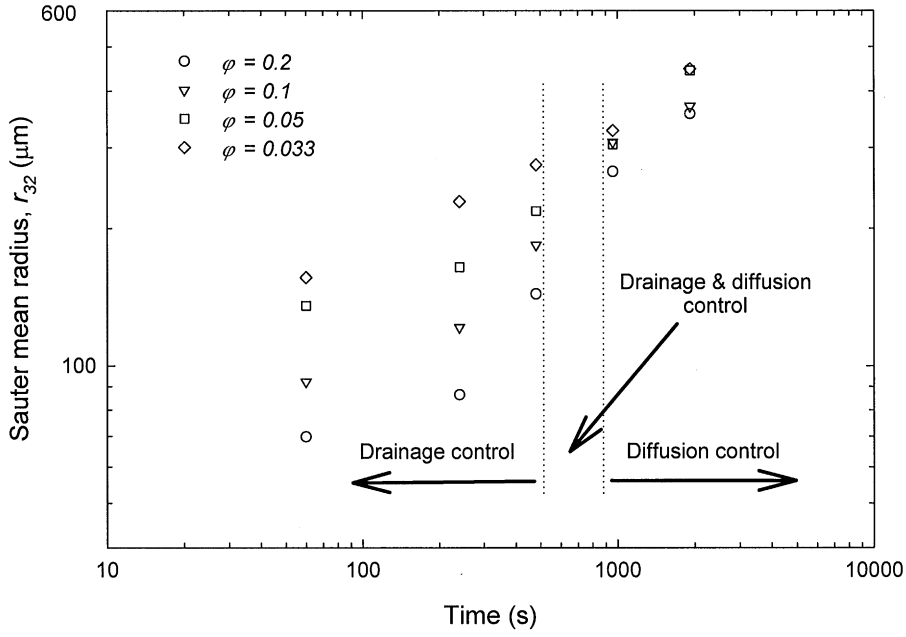

Fig. 9. Bubble growth in compressed-air foams of varying liquid fraction. The evolving foam exhibited three growth regimes, the first 500 s where the bubble growth was controlled by drainage, the second phase showing both diffusion and drainage control and the third phase after 900 s where the bubble growth was governed only by diffusion.

The empirical results for bubble growth in foams in terms of the Sauter mean radius r_{32} are shown in Fig. 9. It is evident that the mean bubble radius increases in the first 500 s after the foam is generated and continues to increase throughout the experiment. Furthermore, the rate of bubble growth is markedly slower after 900 s. These observations can be attributed to a number of factors. Previous studies by Magrabi et al. (1997) have shown that during the initial 500 s of foam aging, drainage plays a dominant role in the instability of foam, in comparison to the other instability mechanisms discussed previously (i.e. coalescence and coarsening). It should be noted that the foams under study were stabilised by using a glycol stabiliser to reduce the coalescence between bubbles. Moreover, no coalescence was observed on viewing the video recordings of the foam. In the later phase of the experiment, namely after 900 s, the drainage rate in the foam sample decreases substantially and the foam reaches the 'scaling state'. The coarsening coefficients exhibited by the foams under study are presented in Table 3 along with the bubble growth exponents obtained in previous experimental and numerical investigations. In all, the evolving foam exhibited three growth regimes: the first 500 s where the bubble growth was controlled by drainage, the second phase showing both diffusion and drainage control and the third phase after 900 s where the bubble growth was governed only by diffusion.

Recent theories on coarsening as well as computer simulations of cellular systems have confirmed the existence of a scaling regime exhibiting a coarsening coefficient of around 0.5. Durian et al. (1991) reported that in a three-dimensional foam the average bubble size increases with time as t^{χ} during the coarsening phase, where $\chi = 0.45 \pm 0.05$. Stavans (1990) observed that for soap bubbles confined between glass plates, coarsening closely follows $t^{0.5}$ if the excess liquid draining from the foam is periodically removed to keep the widths of the Plateau borders constant. Recently, Fortes et al. (1998) reported a coarsening coefficient of 0.54 for a liquid foam of density 0.03 g cm^{-3}.

Table 3
Scaling parameter χ for foam coarsening

System	χ	Reference
Empirical $\varphi = 0.2$	0.55 ± 0.08	Current study
Empirical $\varphi = 0.05$	0.52 ± 0.08	Current study
Empirical-shaving foam (3-D)	0.45 ± 0.05	Durian et al. (1991)
Empirical-soap froths (drained)	0.5	Stavans (1990)
Empirical-foam (0.03 g cm^{-3})	0.54	Fortes (1998)
Computer simulation $\varphi = 0.2$	0.52 ± 0.05	Current study
Computer simulation $\varphi = 0.05$	0.56 ± 0.06	Current study
Computer simulation	0.5–0.6	Herdtle and Aref (1991)
Computer simulation (2-D & 3-D)	0.4 ± 0.1	Gardiner (1998c)
Computer simulation	0.5	Patzek (1993)

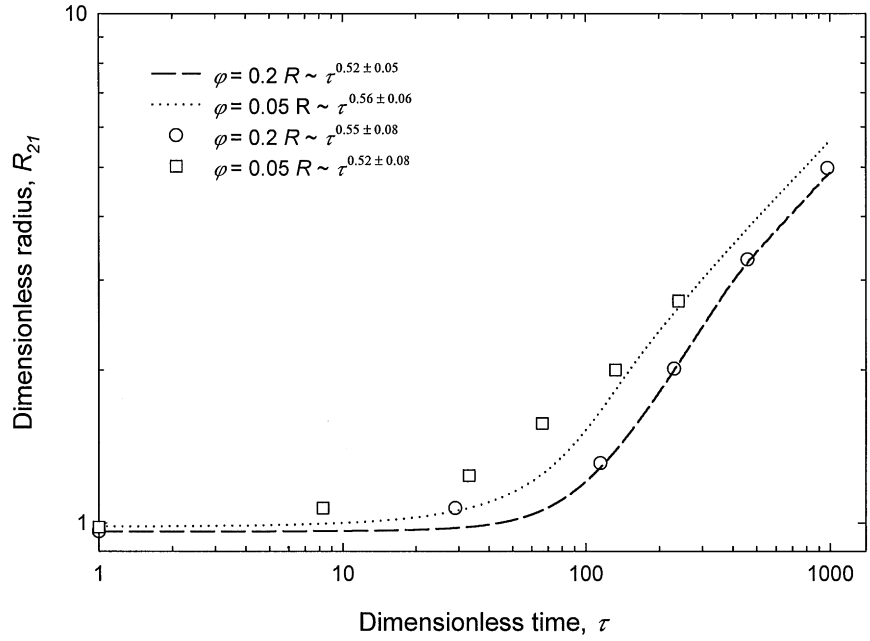

Fig. 10. An illustration of the 'scaling regime' in wet and dry foams. The lines indicate the computer-simulated coarsening while the symbols show the empirical results.

Fig. 10 shows a comparison of the empirical and computer-simulated predictions of bubble coarsening in a wet ($\varphi = 0.2$) and a drier ($\varphi = 0.05$) foam. The onset of the scaling region was deemed to begin after 960 s which corresponds to a dimensionless time $\tau = 555$ for the wet foam ($\varphi = 0.2$) and $\tau = 160$ for the drier foam ($\varphi = 0.05$); see Eq. (11) for the calculation of τ. Empirically, the wet ($\varphi = 0.2$) and drier foams ($\varphi = 0.05$) showed $\chi = 0.55 \pm 0.08$ and $\chi = 0.52 \pm 0.08$, respectively, in the scaling state, which is in satisfactory agreement with previous experimental studies. In the scaling state, the computer simulations demonstrate that coarsening follows $t^{0.52 \pm 0.05}$ in the wet foam and $t^{0.56 \pm 0.06}$ in the drier foam. Moreover, our computer predictions show good agreement with the present empirical observations.

Table 3 also shows the growth exponents for foams obtained via computer modelling in previous studies. Herdtle and Aref (1991) obtained $0.5 < \chi \leqslant 0.6$ for a two-dimensional polygonal foam whilst ignoring liquid drainage and assuming constant lamella permeability. Under similar conditions, Gardiner (1998c) obtained $\chi = 0.4 \pm 0.1$ in two- and three-dimensional foam models, respectively. Patzek's (1993) numerical simulation of a two-dimensional foam gave $\chi = 0.5$ for a foam sample in which the excess liquid (draining from the foam) is not allowed to accumulate at the bottom of the foam sample. A more detailed review of foam coarsening entailing experimental and computer-simulated studies can be found in the paper by Glazier and Weaire (1992).

A convenient means of comparing the empirical and simulated bubble profiles in Figs. 7 and 8 is to analyse them in conjunction with Fig. 10. Fig. 10 shows the empirically measured mean radius R_{21} at $t = 0$, 60, 240, 480, 960 and 1920 s, respectively, plotted in dimensionless coordinates. In the case of the wet foam ($\varphi = 0.2$), the experimental results are more or less consistent with the computer simulation except at $t = 60$ s where the model underpredicts the observed bubble profiles. In the drier foam ($\varphi = 0.05$), the model underpredicts at all instances except at $t = 960$ and 1920 s. The inconsistency can be attributed to experimental and sampling errors (approximately $\pm 15\%$) associated with bubble size measurement.

5. Sensitivity analysis

The bubble-size distribution functions predicted by this model are extremely sensitive to the modelling parameter κ in Eq. (11), which is a function of the effective permeability to gas transfer J. Hence, any parameter that alters the value of κ indirectly affects the evolution of the bubble size distribution predicted by our model. In the following sections, the sensitivity of the model to some of these parameters is examined in detail.

5.1. Product of the gas diffusivity and Henry's constant (D·H)

The equilibrium relationship between the partial pressure of the solute in the gas phase and the concentration in the liquid phase is given by Henry's law. Henry's

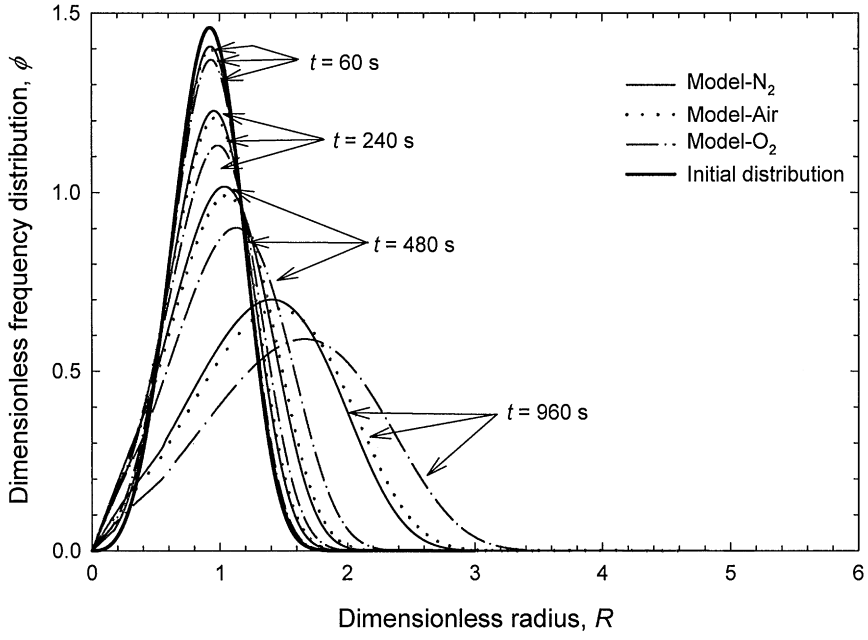

Fig. 11. Model sensitivity to the $D{\cdot}H$ product. The plot illustrates the effect on the simulated bubble size profiles when nitrogen, oxygen or air is used as the gaseous agent respectively to model the drier foam ($\varphi = 0.05$). The predicted bubble distribution functions for nitrogen, oxygen and air are shown at 60, 240, 480 and 960 s, respectively.

law can be re-written for gas diffusion between two bubbles as

$$C_1 = Hp_1, \tag{14}$$

$$C_2 = Hp_2, \tag{15}$$

where C_1 and C_2 are the equilibrium concentrations in the liquid phase and the corresponding equilibrium partial pressures in the gas phase are given by p_1 and p_2. Furthermore, the driving force for gas diffusion between the two bubbles is given by

$$\Delta C = C_1 - C_2 = H(p_1 - p_2) = H\Delta P. \tag{16}$$

Since inter-bubble gas transfer is dependent on both the gas diffusivity and the Henry's constant, the $D{\cdot}H$ product can be utilised as a measure of the mass transfer properties of the gas used in the foam. Fig. 11 shows the sensitivity of the model to the $D{\cdot}H$ product of the various gases listed in Table 4. It collates the bubble size distribution predicted by the model for foams generated by using pure oxygen, pure nitrogen and air. Oxygen has a relatively higher solubility and diffusivity in water than nitrogen, resulting in a dramatic increase in the coarsening rate of the foam generated using pure oxygen. In effect, the model is sensitive to the $D{\cdot}H$ product of the gas used in the foam. For simulation purposes, we used properties of pure water and expect that the use of values of the diffusivity and Henry's constants for air in the foam solution (3% foam concentrate–97% water) would produce improved agreement between the model predictions and the experimental results. The model utilised in this study is a binary diffusion model of N_2 diffusing through a stationary liquid, when in reality the aerated foams exhibit multi-component diffusion, with N_2 and O_2 diffusing at different rates. In addition, the gas diffusivity D affects the calculation of the dimensionless time τ in the model; see Eq. (11). Therefore, any alteration of the gas diffusivity introduces an uncertainty into the model predictions.

Table 4
Tabulation of D·H product for nitrogen, air and oxygen in water

	N_2	Air	O_2
D (m^2 s)[a]	1.90×10^{-9}	2.02×10^{-9}	2.50×10^{-9}
H (mol m^{-3} Pa^{-1})[b]	6.65×10^{-6}	7.66×10^{-6}	1.26×10^{-5}
$D{\cdot}H$	1.26×10^{-14}	1.55×10^{-14}	3.15×10^{-14}

[a] Perry and Green (1984).
[b] International Critical Tables, vol. 5.

5.2. Surface tension

Coarsening in foams results' in the net increase in the average bubble size over time. It is ultimately driven by surface tension and serves to decrease the total interfacial area with time. Moreover, the surface tension also affects drainage. Therefore, surface tension has a profound effect on the working of this model. The sensitivity of the simulations to surface tension is illustrated in Fig. 12. Ideally, the foam solution is composed of 3% foam concentrate–97% water with $\sigma = 0.0225$ N/m. The plot

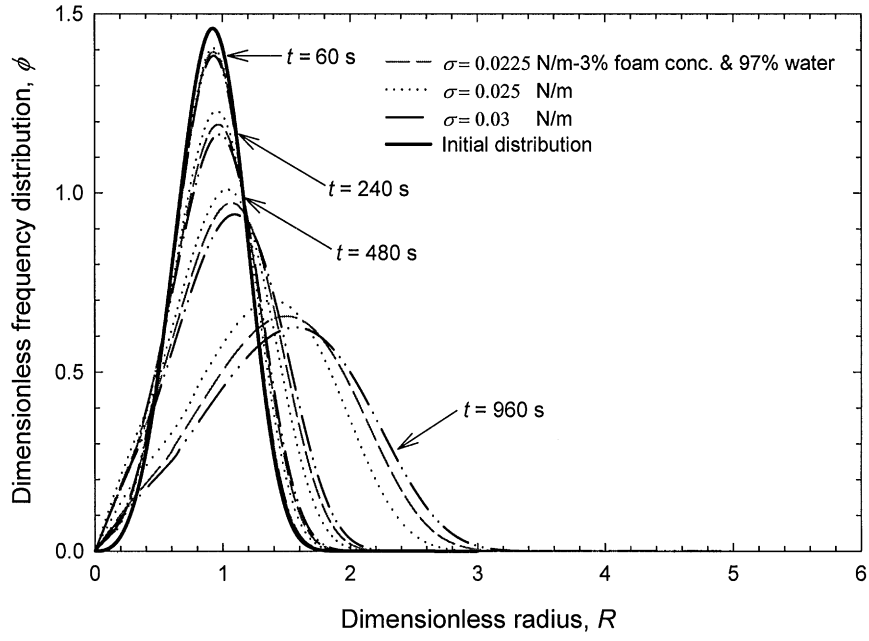

Fig. 12. A contrast in the resulting bubble size distribution when the surface tension of the foam solution is altered in the drier foam ($\varphi = 0.05$). Ideally, the foam solution is composed of 3% foam concentrate–97% water with $\sigma = 0.0225$ N/m. The plot illustrates the predicted bubble distribution functions at 60, 240, 480 and 960 s, respectively, when σ is increased to 0.025 or 0.03 N/m, respectively. The coarsening rate increases with an increment in the surface tension.

illustrates the sensitivity of the model when σ is increased to 0.025 or 0.03 N/m, respectively. The coarsening rate increases with an increment in the surface tension.

5.3. Volume fraction of liquid

The inclusion of drainage effects (i.e. variation of liquid fraction with time) in the bubble growth model, has a marked effect on the prognosis of bubble size profiles with time. This can be readily inferred from the difference in the modelled bubble distribution functions (see Figs. 5 and 7). In effect, this shows that the simulated bubble size profiles have a high degree of sensitivity to the liquid fraction present in the foam.

The sonic velocity method used to empirically measure the change in the liquid fraction in the foam was estimated to have an uncertainty of $\pm 10\%$. Fig. 13 demonstrates the sensitivity of the model when an uncertainty of $\pm 10\%$ is included in the liquid fraction profiles in Fig. 6. A negative shift of 10% in the liquid fraction profile in Fig. 6 retards the coarsening process, while a positive shift of 10% in the liquid fraction profile accelerates the coarsening process. Effectively, this implies that due to drainage effects a drier foam coarsens more slowly than a wet foam.

5.4. Other factors

All the parameters outlined previously are temperature and pressure dependent, thereby introducing an additional uncertainty in the computer simulations. By combining all the above factors, the overall uncertainty in the predictions from the model is estimated to be $\pm 10\%$.

While our model incorporates the drainage of liquid and inter-bubble gas diffusion during the aging of foams, the effect of coalescence on foam decay was not considered. In practice, the occurrence of coalescence can be eliminated. This was accomplished in our study by using a glycol stabiliser to stabilise the foam; refer to Table 1. The absence of coalescence was verified by viewing the experimental recordings of the foam under study.

The bubble size profiles predicted by this model show excellent agreement with the empirical observations. The model used in the present study assumes that during inter-bubble gas diffusion, the gas is transferred from the bubbles (whose radius is less than the mean radius) to the liquid in the adjoining films and Plateau border. The liquid then redistributes the gas to the bubbles whose radii exceed the mean radius. In the dry limit ($\varphi \to 0$), when the film thickness reaches a steady state and the liquid in the films is reduced to a minute quantity, diffusion occurs directly between adjacent bubble pairs. Therefore the model is not expected to yield reliable results in the dry limit. Another limitation of our model, is the inability to predict the growth of dislocations or defects in foams, such as a dislocation caused by a large bubble in an otherwise uniform bubble size foam.

A number of models have been developed lately to simulate bubble growth in foams in two dimensions (Bolton and Weaire, 1990; Glazier et al., 1990; Herdtle

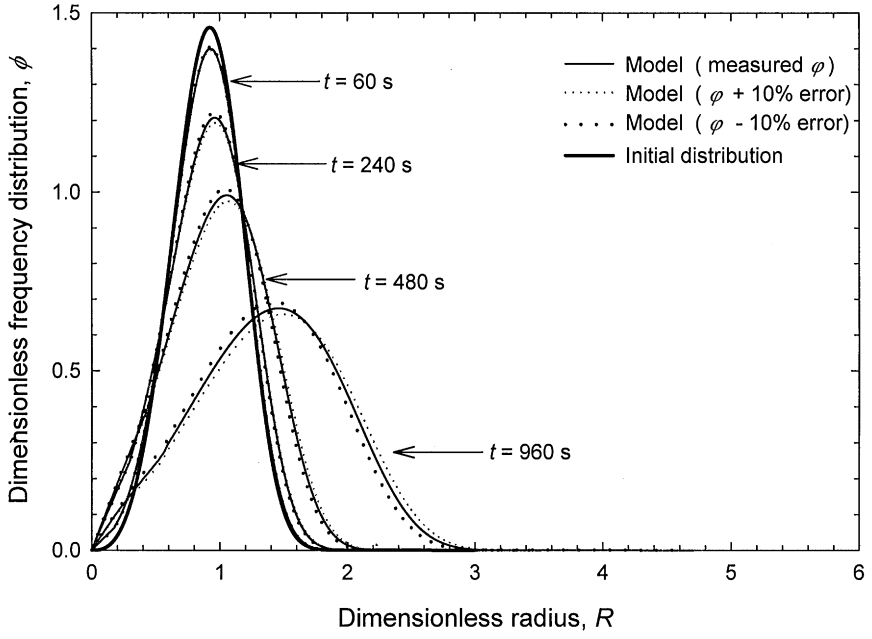

Fig. 13. Model sensitivity to liquid fraction, illustrated by the predicted bubble distribution functions at 60, 240, 480 and 960 s, respectively, in the drier foam ($\varphi = 0.05$). A negative shift of 10% in the liquid fraction profile in Fig. 7 retards the coarsening process, whilst, a positive shift of 10% in the liquid fraction profile accelerates the coarsening process.

and Aref, 1991; Patzek, 1993) and in three dimensions (Avron and Levine, 1992; de Almeida and Mombach, 1997). However, most of these studies concentrate on simulating dry foams in their 'scaling state' and only a few consider the effect of liquid drainage and the resulting changes in the lamella thickness. In addition, these models encompass both diffusional adjustments and topological transitions during foam coarsening. The approach used to model bubble growth in this study, takes into account any diffusive adjustments in the foam along with the change in the lamella thickness with time (due to drainage) and does not predict topological alterations during the aging process.

6. Conclusions

This paper encompasses empirical and theoretical approaches to the analysis of bubble growth in compressed-air foams. Compressed-air foams are characterised by a narrower bubble size distribution than gas-aspirated foams used in previous studies. Contrary to the log-normal bubble distribution observed in gas-aspirated foams, compressed-air foams exhibit Weibull-type distributions.

Recent empirical studies as well as direct computer simulations of cellular systems have confirmed the existence of a scaling regime exhibiting a coarsening coefficient of around 0.5. Our experimental and computer simulated coarsening coefficients show good agreement with previous studies.

In this work, we have extended Lemlich's (1978) model by incorporating the change in liquid fraction, due to drainage, as the foam ages. This extension enables the simulation of coarsening and the time evolution of bubble size distribution functions. A number of models have been developed lately to simulate bubble growth in foams. However, a majority of these studies concentrate on simulating dry foams in their 'scaling state' and do not consider the effect of liquid drainage and the resulting changes in the film thickness. In practical applications the drainage controls the initial coarsening of the foams and must be taken into account.

The bubble size distribution functions predicted by this model show excellent agreement with the empirical observations, for both wet and drier foams. A sensitivity analysis indicated a significant dependence of the model on drainage (hence on the thickness of the lamellae), Henry's constant, diffusivity and surface tension. An error analysis on the model estimated an uncertainty of around 10% in the results from the computer simulations.

Acknowledgements

This study was funded by the Australian Research Council and by a student grant from the Society of Fire Protection Engineers (SFPE). The authors wish to thank Mr Ted Schaefer of 3M Australia for developing a generic formulation of class B foam concentrate used in this study. In addition, we acknowledge useful

correspondence with Emeritus Professor Robert Lemlich of the University of Cincinnati.

Notation

C	molar concentration, mol m^{-3}
C_p	heat capacity at constant pressure, m^2 s^{-2} K
C_v	heat capacity at constant volume, m^2 s^{-2} K
CAF	compressed-air foams
CCD	charge-coupled device
d_b	area-equivalent diameter, m
D	diffusivity of the gaseous component in the liquid phase, m^2 s^{-1}
f	film thickness, m
f_s	frequency distribution function in the foam at the transparent surface, dimensionless
$F(r)$	frequency distribution function in the bulk of the foam, dimensionless
h	interfacial resistance to mass transfer, mol s kg^{-1} m^{-1}
H	Henry's constant in terms of solubility, mol m^{-3} Pa^{-1}
J	effective permeability to gas transfer, mol s kg^{-1} m^{-1}
K	parameter $[2J\sigma R_g T/P_a]$, m^2 s^{-1}
n	moles of gas in a bubble, mol
$\dot{n}$	molar diffusion rate, mol s^{-1}
n_i	number of bubbles of radius r in the foam, dimensionless
p	partial pressure, Pa
P_a	atmospheric pressure, Pa
r	bubble radius, m
r_{10}	mean radius defined by the first moment, m
r_{21}	mean bubble radius defined by the second and first moments, m
r_{32}	mean bubble radius defined by the third and second moments, m
r_i	initial arithmetic mean radius, m
R	dimensionless radius ($= r/r_c$)
R_g	universal gas constant, N m gmol^{-1} K^{-1}
t	time, s
T	temperature, K
v	sonic velocity in foam, m s^{-1}
x	mole fraction of the species
z	diffusional path length, m

Greek letters

α	statistical distribution parameter for Weibull distribution, dimensionless
β	statistical distribution parameter for Weibull distribution, dimensionless
γ	ratio of specific heats ($= C_p/C_v$), dimensionless
δ	radius of virtual bubble, m
κ	dimensionless parameter ($= K/D$)
ρ_l	density of foam solution, kg m^{-3}
σ	surface tension, N m^{-1}
τ	dimensionless time ($= t/(r_c^2/D)$)
ϕ	dimensionless frequency distribution function
φ	volume fraction of liquid in the foam
χ	coefficient of coarsening
ψ	rate of bubble growth, m s^{-1}

Appendix

In his model for inter-bubble gas diffusion, Lemlich (1978) proposed the following pathway for inter-bubble gas transfer; see Fig. A.1. The gas diffuses from the bubbles to the liquid region midway between adjacent bubbles, and then from the liquid to all bubbles. For a dilute gas A ($x_A \ll 1$) diffusing through a stationary liquid B, $N_B \cong 0$, Fick's law reduces to

$$N_A = -CD\frac{\mathrm{d}x_A}{\mathrm{d}z} = -D\frac{\mathrm{d}C_A}{\mathrm{d}z}. \tag{A.1}$$

For dilute solutions, the concentration of gas A at the boundary can be expressed in terms of its partial pressure in the gas phase, by using Henry's law as

$$C_1 = Hp_1^i. \tag{A.2}$$

Inserting Eq. (A.2) into Eq. (A.1) and re-writing Eq. (A.1) to represent mass transfer between two bubble interfaces gives

$$N_A = -DH\frac{p_2^i - p_1^i}{\Delta z}. \tag{A.3}$$

If we assume that the transfer of gas takes place between bubble 1 and a virtual bubble V located midway between bubbles 1 and 2, then $\Delta z = f/2$ and Eq. (A.3) becomes

$$-\frac{N_A f}{2DH} = p_V - p_1^i. \tag{A.4}$$

The molar transfer of gas A from bubble 1 to the interface can be represented as

$$N_A = h(p_1 - p_1^i) \quad \text{or} \quad -\frac{N_A}{h} = (p_1^i - p_1), \tag{A.5}$$

where h denotes the surface mass transfer coefficient. Summing Eqs. (A.4) and (A.5) yields

$$N_A = -\frac{p_V - p_1}{(1/h) + f/2DH} = -J\Delta P, \tag{A.6}$$

where

$$\frac{1}{J} = \frac{1}{h} + \frac{f}{2DH}, \tag{A.7}$$

as indicated in Eq. (9) of this paper.

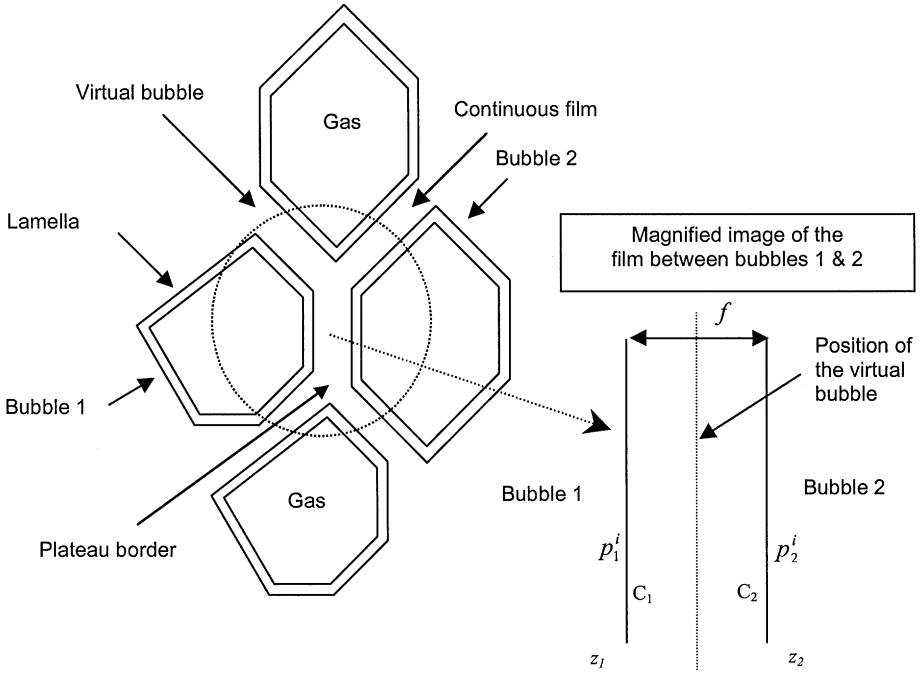

Fig. A.1. Schematic illustrating the development of the Lemlich (1978) model.

By applying the Laplace–Young law, the pressure in the liquid region can be assigned to that of a virtual bubble having radius of curvature δ, located midway between adjacent real bubbles. Therefore, the pressure difference between a bubble, having radius of curvature r_c, and the liquid can be written as

$$\Delta P = 2\sigma\left(\frac{1}{\delta} - \frac{1}{r_c}\right), \tag{A.8}$$

where σ denotes the surface tension and ΔP can be positive or negative. Although, foam bubbles have a polyhedral shape, the radius of curvature r_c of the bubbles were approximated by the spherical bubble radius r.

Eq. (A.6) can be expressed as

$$\dot{n} = -JA\Delta P, \tag{A.9}$$

where $\dot{n} = N_A A$. By approximating the surface area for mass transfer between the bubbles by $4\pi r^2$ and combining Eqs. (A.8) and (A.9) we obtain

$$\dot{n} = 8\pi J\sigma\left(\frac{r^2}{\delta} - r\right). \tag{A.10}$$

By assuming conservation of gaseous moles in the entire foam and summing over all the bubbles, Eq. (A.10) yields

$$\sum n_i\left(\frac{r^2}{\delta} - r\right) = 0, \tag{A.11}$$

where n_i is the number of bubbles of radius r in the foam. An effective average radius δ denotes the size of the virtual bubble which varies with time t yielding

$$\delta = \frac{\int_0^\infty r^2 F(r,t)\,\mathrm{d}r}{\int_0^\infty rF(r,t)\,\mathrm{d}r} \tag{A.12}$$

where $F(r,t)$ is the frequency distribution function of r at t. Eq. (A.12) follows directly from Eq. (A.11) and is equivalent to the mean radius given by the second and first moments of a distribution r_{21}. Under normal circumstances, the pressure in a bubble is only slightly higher than the ambient pressure P_a. Hence, the pressure in a bubble is approximated by the atmospheric pressure, and the ideal gas law yields the following relationship for the moles of gas n in a bubble:

$$n \approx \frac{4\pi P_a r^3}{3R_g T}. \tag{A.13}$$

By combining Eqs. (A.11)–(A.13), the rate at which the bubble radius at time t changes with time is given by

$$\psi(r,t) = \frac{\mathrm{d}r}{\mathrm{d}t} = \frac{2J\sigma R_g T}{P_a}\left(\frac{\int_0^\infty rF(r,t)\,\mathrm{d}r}{\int_0^\infty r^2F(r,t)\,\mathrm{d}r} - \frac{1}{r}\right). \tag{A.14}$$

References

Avron, J.E., & Levine, D. (1992). Geometry and foam-2D dynamics and 3D statics. *Physical Review Letters*, *69*, 208–211.

Bikerman, J.J. (1973). *Foams*. New York: Springer.

Bisperink, C.G.J., Ronteltap, A.D., & Prins, A. (1992). Bubble size distribution in foams. *Advances in Colloid and Interface Science*, *38*, 13–32.

Bolton, F. and Weaire, D. (1990). Rigidity loss transition in a disordered 2D foam. *Physical Review Letters*, *65* (27), 3449–3451.

Calvert, J.R., & Nezhati, K. (1986). Bubble size effects in foams. *International Journal of Heat Fluids*, *8*, 102–106.

Cheng, H.C., & Lemlich, R. (1983). Errors in the measurement of bubble size distribution in foam. *Industrial and Engineering Chemistry Fundamentals*, *38*, 105–109.

de Almeida, R.M.C., & Mombach, J.C.M. (1997). Scaling properties of three-dimensional foams. *Physica A*, *236*, 268–278.

de Icaza, M., Jimenez-Ceniceros, A., & Castano, V.M. (1994). Statistical distribution functions in 2-D foams. *Journal of Applied Physics*, *76* (11), 7317–7321.

de Vries, A.J. (1957). *Foam stability*. Delft: Rubber-Stichting.

de Vries, A.J. (1972). In: R. Lemlich (Ed.), *Absorptive bubble separation techniques* (pp. 7–30). New York: Academic Press.

Durian, D.J., Weitz, D.A., & Pine, D.J. (1991). Scaling behaviour in shaving cream. *Physical Review A*, *44*, 7902–7905.

Fortes, M.A., Rosa, E.M., Findlay, S., & Guedes, M. (1998). Development of bamboo structure in a foam: The kinetics of foam coarsening. *Philosophical Magazine A*, *77* (1), 257–265.

Gal-Or, B., & Hoelscher, H.E. (1966). A mathematical treatment of the effect of particle size distribution on mass transfer in dispersions. *The American Institute of Chemical Engineers Journal*, *12*, 499–508.

Gandolfo, F.G., & Rosano, H.L. (1997). Interbubble gas diffusion and the stability of foams. *Journal of Colloid and Interface Science 194*, 31–36.

Gardiner, B.S., Dlugogorski, B.Z., & Jameson, G.J. (1998a). Rheology of fire-fighting foams. *Fire Safety Journal*, *31* (1), 61–75.

Gardiner, B.S., Dlugogorski, B.Z., & Jameson, G.J. (1998b). Yield stress measurements of aqueous foams in the dry limit. *Journal of Rheology*, *42* (6), 1437–1450.

Gardiner, B.S. (1998c). Personal communication.

Glazier, J.A., Andersen, M.P., & Grest, G.S. (1990). Coarsening in two dimensional soap froths and the large-Q Potts model: A detailed comparison. *Philosophical Magazine A*, *62* (6), 615–645.

Glazier, J.A., & Weaire, D. (1992). The kinetics of cellular patterns. *Journal of Physics*: *Condensed Matter*, *4*, 1867–1894.

Herdtle, T., & Aref, H. (1991). Relaxation of fractal foam. *Philosophical Magazine Letters*, *64* (5), 335.

Himmelblau, D.M. (1970). *Process analysis by statistical methods*. New York: Wiley.

International critical table of numerical data, Physics, Chemistry and Technology (1929). E.W. Washburn, Editor, McGraw-Hill, New York.

Kroezen, A.B.J., & Wassink, J.G. (1987). Bubble size distribution and energy dissipation in foam mixers. *Journal of the Society of Dyers and Colourists*, *103*, 386–394.

Lachaise, J., Sahoun, S., Dicharry, C., & Salager, J.L. (1991). Improved determination of the initial structure of liquid foams. *Progress in Colloid and Polymer Science*, *84*, 253–256.

Lemlich, R. (1978). Prediction of changes in bubble size distribution due to interbubble gas diffusion in foam. *Industrial and Engineering Chemistry Research*, *17* (2), 89–93.

Lemlich, R. (1982). A Boltzmann-like model for the size distribution of bubbles or droplets in a well mixed dispersion. *Chemical Engineering Communications*, *16*, 153–157.

Lewis, D.A., Nicol, R.S., & Thompson, J.W. (1984). Measurement of bubble sizes and velocities in gas-liquid dispersions. *Chemical Engineering Research Design*, *62*, 334–336.

Liebson, J. (1991). *Introduction to class A foams and compressed air systems for the structural fire service*. Ashland, MA: ISFSI.

Magrabi, S.A., Dlugogorski, B.Z., & Jameson, G.J. (1997). Attenuation of thermal radiation by aqueous foams. *Proceedings of the 24th Australia and New Zealand Chemical Engineering Conference*, Rotorua, New Zealand, 29 September–1 October, SF2a: 319.

Manegold, E. (1953). *Schaum*. Heidelberg: Chemie und Technik Verlagsgesellschaft.

Markworth, A.J. (1985). Comments on foam stability, Ostwald ripening and grain growth. *Journal of Colloid and Interface Science*, *107* (2), 569–571.

Monsalve, A., & Schechter, R.S. (1984). The stability of foams: Dependence of observation on the bubble size distribution. *Journal of Colloid and Interface Science*, *97* (2), 327–335.

NFPA-412 (1993). *Standard for evaluating aircraft rescue and fire-fighting foam equipment*. National Fire Protection Association, Quincy, MA.

Patzek, T.W. (1993). Self-similar collapse of stationary bulk foams. *The American Institute of Chemical Engineers Journal*, *39* (10), 1697–1707.

Perry, R.H., & Green, D. (1984). *Perry's chemical engineers hand book* (6th ed.). USA: McGraw-Hill.

Rand, P.B., & Kraynik, A.M. (1983). Drainage of aqueous foams: Generation-pressure and cell size effects. *Society of Petroleum Engineers Journal 23* (1), 152–154.

Sarma, S.R., & Khilar, K.C. (1988). Effects of initial gas volume fraction on stability of aqueous air foams. *Industrial and Engineering Chemistry Research*, *27* (5), 892–894.

Stavans, J. (1990). Temporal evolution of two-dimensional drained soap froths. *Physical Review A*, *42* (8), 5049–5051.

Tam, W.Y., Zeitak, R., Szeto, K.Y., & Stavans, J. (1997). First-passage exponent in two-dimensional soap froths. *Physical Review Letters*, *78* (8), 1588–1591.

Von Neumann, J. (1952). *Metal interfaces*. Cleveland, OH: American Society of Metals.

Weibull, W. (1951). A statistical distribution function of wide applicability. *Journal of Applied Mechanics*, *18(3)*, 293–297.

Wood, A.B. (1941). *A textbook of sound*. London: Bell.